Experimental Flow Analysis in a Modern Turbine Rear Structure with 3D Polygonal Shroud Under Realistic Flow Conditions

EXPERIMENTAL FLOW ANALYSIS IN A MODERN TURBINE REAR STRUCTURE WITH 3D POLYGONAL SHROUD UNDER REALISTIC FLOW CONDITIONS

V. Vikhorev, V. Chernoray

Chalmers University of Technology, Gothenburg, Sweden
valvik@chalmers.se, valery.chernoray@chalmers.se

ABSTRACT

Continuous advancement of the existing design of turbine rear structure (TRS) leads to new challenges in terms of aerodynamic efficiency. This work presents experimental aero studies of the effect of the 3D polygonal shroud in the TRS comprising several types of guide vanes representative of a modern TRS: regular vanes, thickened vanes, and vanes with a mount bump. The experiments were performed in an engine-realistic facility for a fixed Reynolds number, 350000, and three operation points based on a low-pressure turbine (LPT) exit swirl angle. The current study shows that the thickened vane handles the on-design and off-design conditions with good aerodynamic performance. It is observed that a shroud bump significantly affects the pressure losses because of the additional vorticity region created from the bump itself, and it has an upstream influence on the outlet flow from the LPT.

KEYWORDS

TURBINE REAR STRUCTURE, TURBINE EXHAUST CASING, LOW-PRESSURE TURBINE, OUTLET GUIDE VANE, OUTLET MOUNT RECESS

NOMENCLATURE

C_{p0}	*total pressure coefficient,* $(P_t–P_{t,ref})/(P_{t,ref}–P_{s,ref})$
C_p	*static pressure coefficient,* $(P_s–P_{s,ref})/(P_{t,ref}–P_{s,ref})$
FC	*flow coefficient, Ux/V*
H	*channel height at inlet, m*
PS	*pressure side*
P_s	*static pressure, Pa*
P_t	*total pressure, Pa*
Re	*Reynolds number,* U_xH/v
SS	*suction side*
V	*blade velocity, m/s*
U_x	*axial flow velocity, m/s*
x	*streamwise coordinate, m*
v	*kinematic viscosity,* m^2/s
Θ	*angular coordinate, deg*

INTRODUCTION

One of the main challenges of current air transport systems is aimed at achieving resource-efficient, climate- and environmental-friendly level. In compliance with this requirement, including the global environmental targets such as reduction of fuel consumption, carbon dioxide emissions and relative to the engine noise, modern geared turbofan engines are being developed.

Enabling the fan and turbine to rotate at different speeds provided by geared turbofan engines significantly increases the by-pass ratio and, therefore, the propulsive efficiency. At the same time the swirl angles from the last low-pressure turbine (LPT) rotor to the turbine rear structure (TRS) can be kept lower. However, with geared engines the off-design variations of the outlet swirl angle increases,

which makes it more aerodynamically challenging to design TRS with built-in outlet guide vanes (OGV) to recover the swirl flow and increase the thrust for all operating points of the turbine.

In addition, modern turbofan engines must satisfy all structural and engineering requirements of the engine. Therefore, state-of-the-art TRS often requires a three-dimensional polygonal shape and comprises several vane types: regular vanes, thickened vanes with additional space for bearing oil pipelines, and vanes with mount bumps for attachment to the engine. From the perspective of aerodynamics, such engine-relevant modifications for shroud geometry as well as vane geometry can affect the development of end-wall boundary layers or even triggers possible flow separations, thereby, increasing pressure losses. Therefore, TRS development is directly related to the need for its aerodynamic investigation.

Because of the lower cost and easier implementation, the annular arrangement of a TRS blade row is often simplified by a linear arrangement. Therefore, the first experimental investigations of the secondary flow development were carried out by Hjärne et al. (2006) in a linear cascade, providing insight into the interaction of boundary layers coming from OGV, hub and shroud in TRS. In further work by Hjärne et al. (2007), numerical validation of secondary flow evolution was performed. In addition, to deepen the analysis for the turbulence models, the authors also considered the effect of secondary flows on the downstream losses. Sonoda et al. (2008) compared two alternatively designed cascades and provided new insight on the flow mechanisms around the end-wall region. However, two-dimensional approximation of vanes suffers from weaknesses such as lack of possibility to simulate radial pressure gradients and limited flow periodicity.

Regarding the problems mentioned above, the annular cascade reproduces the flow conditions more realistically than a linear cascade. Selic et al. (2012) were the first to investigate the effect of the leakage flow on the flow structure of the OGV in an annular rig with an unshrouded turbine. Radial variation in swirl, total pressure and yaw angle over the passage height as well as three-dimensional effects were investigated by Schönleiner et al. (2014). Further works were done in an engine-realistic facility with shrouded LPT located at the Chalmers University of Technology. Considerable efforts were made by Jonsson et al. (2019) to measure heat transfer on regular OGVs for several design conditions indicating the laminar-turbulent transition, which is crucial for the TRS performance. More detailed investigation of regular OGV's with additional CFD results can be found in a recent paper written by Jonsson et al. (2020).

Besides, as mentioned above, modern TRS includes several vane types. Therefore, it is crucial to consider the aerodynamic performance of each type of vane and their mutual influence. The influence of the vane with mount bump in the linear cascade was previously studied by Hjärne et al. (2008). In addition, Vikhorev et al. (2020) also carried out aerodynamic studies. They revealed a significant effect of the bump vane on pressure losses in the near-hub region of the OGV and upstream influence on the inlet conditions.

Moreover, the authors performed an oil-film visualization to demonstrate the flow behaviour around OGV's and compared the patterns for the different design conditions. These measurements were done in an annular engine-realistic rig with a circular shroud. However, aerodynamic investigations for the TRS with polygonal shroud geometry have not previously been conducted. Therefore, the main goal of this work is to study the effect of a 3D polygonal shroud design in a modern TRS including several vane types: regular vanes, vanes equipped with bump and vanes with increased thickness to give more internal space for the passage of the bearing oil pipes and scavenge tubes. The engine realistic TRS with all three vane types mounted simultaneously was investigated to consider the mutual influence between the vanes.

EXPERIMENTAL FACILITY AND INSTRUMENTATION

The experimental study of the engine-realistic TRS was conducted in an annular low-speed large-scale 1.5 stage LPT-OGV facility at Chalmers University of Technology, Sweden. The schematic view of the facility is shown in Fig. 1. The airflow driven by a 250-kW centrifugal fan passes through corner ducts and diffusers. After the expansion, the flow enters the settling chamber with stainless

steel screens and honeycomb to remove non-uniformities of the flow. Following this, the flow passes through the contraction and reaches an LPT stage which is required to simulate realistic boundary conditions to the TRS. The LPT stage comprised stator stage with 60 nozzle guide vanes (NGVs) and rotor stage with 72 blades and was designed by GNK Aerospace Engine Systems, Sweden.

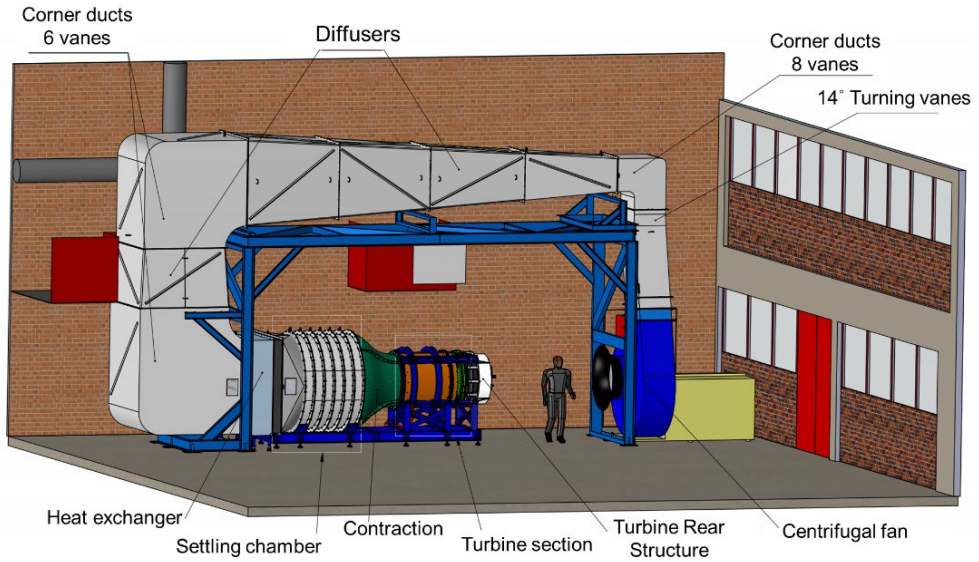

Figure 1: 3D view of the high-Reynolds number continuous operation LPT-OGV facility

The Reynolds number in a TRS of an aero-engine based on channel height and axial velocity ranges from 100000 to 600000 depending on the engine type and size. The flow coefficient (FC), is a second main parameter of the facility, determining the turbine load, and defined as the ratio of the axial velocity to the blade speed:

$$\boldsymbol{FC = U_x/V} \tag{1}$$

The TRS section of the facility is built to be modified and, for the current configuration, designed by GKN Aerospace Engine Systems. It comprises 12 OGVs with a 3D polygonal shroud design (Fig. 2a). It shall be noted that the LPT and TRS components have been designed solely for the experimental rig and are not related to any GKN Aerospace product characteristics.

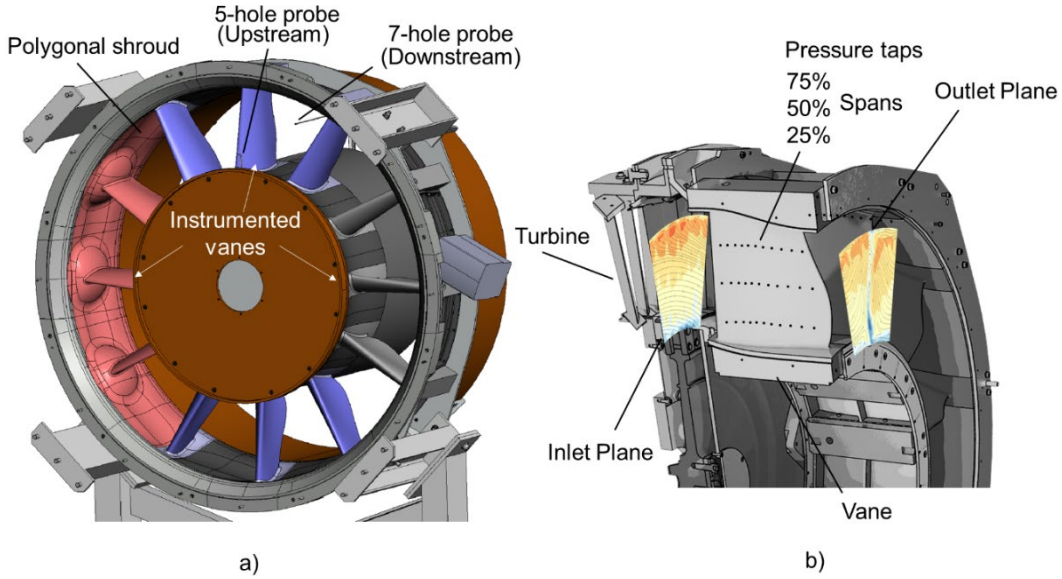

Figure 2: 3D model of tested Turbine Rear Structure

There are two internal traversing systems installed in the TRS section needed to position probes. Both systems are working independently and capable of moving in radial and circumferential directions. Moreover, one traversing system is equipped with an additional motor enabling the downstream probe to be positioned in the axial direction, and therefore, the traversing systems cover near full-volume of the TRS section. The positioning and data acquisition is controlled by a PC with in-house LabVIEW® (National Instruments Corporation, Austin, TX, USA) software scripts. The accuracy of positioning in the circumferential directions is 0.01° while in the radial and axial directions are 0.075 mm.

The total pressure and swirl measurements are accomplished using pre-calibrated 5-hole and 7-hole aero probes, located upstream (Inlet plane) and downstream (Outlet plane) respectively (Fig. 2b). Wall pressure measurements on the vane and shroud bump were done using two Scanivalve mechanical multiplexers with 48 ports each. Acquisition of pressure data was performed using a 16-channel PSI-9116 system with a 500 Hz sampling rate and 2.5 seconds of sampling time. This data was time averaged and only average values were analysed. Pressure values were acquired relative to the total pressure taken from a stationary Prandtl tube located in the bulk flow region between OGVs at 0.7 chord distance from the leading edge.

Furthermore, obtained pressure data were processed and converted to the form of non-dimensional coefficients (Eq. 2 and 3).

$$C_{p0} = \frac{P_t - P_{t,ref}}{P_{t,ref} - P_{s,ref}} \tag{2}$$

$$C_p = \frac{P_s - P_{s,ref}}{P_{t,ref} - P_{s,ref}} \tag{3}$$

Tests are performed at on-design and off-design conditions. The flow Reynolds number of 350000 is used for all three operation points. The flow coefficient values and, respectively, averaged LPT exit swirl angles (the TRS inlet conditions) are summarized in Table 1, where on-design parameters are marked with green.

	Off-design (low loading)	**On-design**	Off-design (high loading)
Flow coefficient	0.555	0.622	0.66
Inlet swirl angle	-6.3	-16.9	-22.4
Reynolds number	350000		

Table 1: TRS inlet conditions

Following the goal of weight reduction, the current configuration consists of 6 thin vanes, called regular vanes. However, the requirement of allowing oil pipelines to pass through OGVs leads to the enlarged thickness of the OGVs. In addition, recent TRS designs require integration of vanes with sunken engine-mount bumps. Therefore, the test section was equipped with three thick vanes and three bump vanes together with six regular vanes.

Figure 3 shows the 3D models of regular, thick and bump OGVs, which were manufactured with SLA rapid prototyping technology. Compared to the regular OGV, the mid-span airfoil section of the thick OGV has an increased thickness by 45% while the camber line was designed the same. The vane surfaces were fitted with pressure taps to measure static pressure distribution and obtain aerodynamic loads. For three spans (25, 50 and 75%) the pressure taps covered pressure and suction sides. For the bump vane, the bump was equipped with extra pressure taps on its surface.

Oil-film visualizations were carried out for the thick and bump vane due to the expected different nature of the flow development. The visualizations were performed using the oil-film technique at different design conditions. A mixture of a mineral oil and TiO2 powder, with particles from 0.2 to 0.3 µm was used. The flow patterns were captured using a digital camera GoPro Hero4.

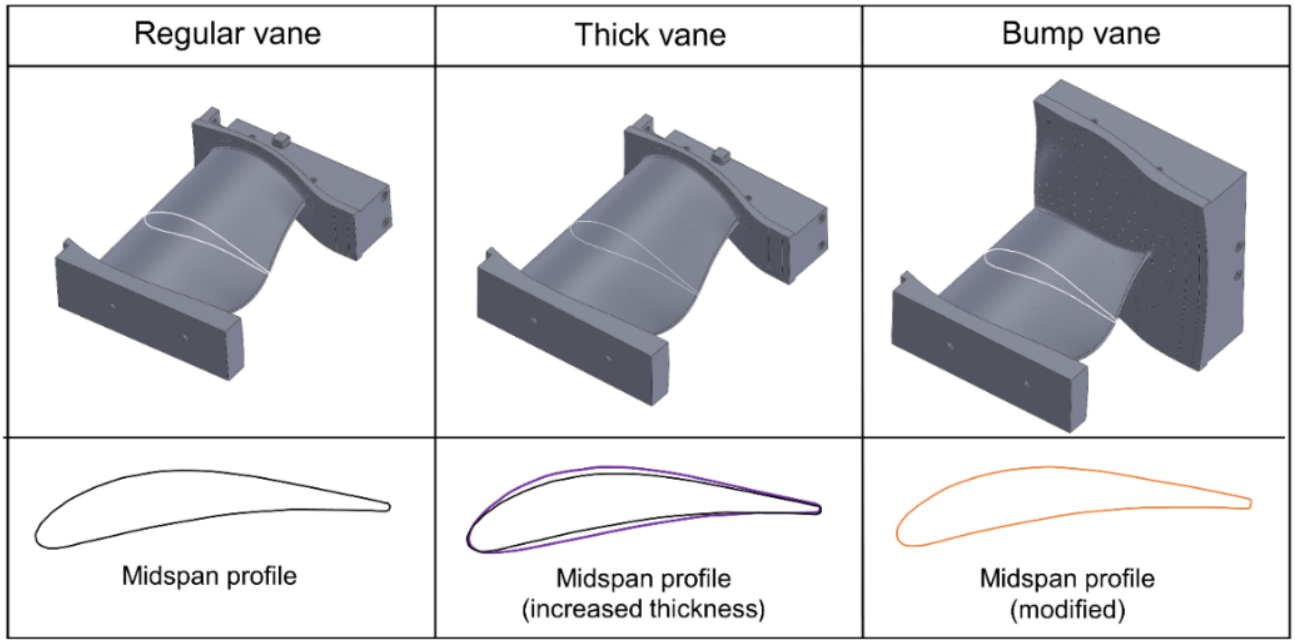

Figure 3: 3D models of regular, thick and bump vanes with their midspan profiles

RESULTS AND DISCUSSION

This section presents the results and discussions concerning the experimental investigations divided into two sections according to the type of measurements. The following results were obtained for the new configuration, including 3D polygonal shroud and three types of vanes: regular, thick and bump vanes.

Pressure measurements

Inlet and outlet measurements

Inlet measurements were performed for a 30-degree sector located upstream of the OGV. The azimuthal resolution was 0.6˚ and radial resolution was 9.7 mm. Figure 4 shows the comparison of upstream total pressure distributions for the regular, thick and bump vane at on-design condition.

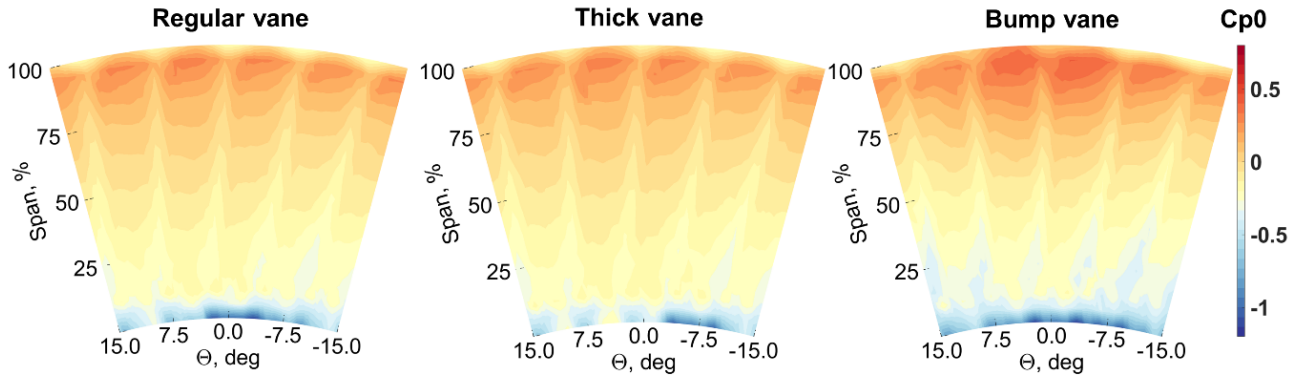

Figure 4: Inlet total pressure coefficient distributions for regular, thick, and bump vanes at on-design condition

Concerning the flow structures coming from the LPT stage, stator wakes developed from NGVs can be observed for all configurations. In addition, the presence of vortex pair developed from each NGV's results in local pressure drop near the hub region. A more detailed explanation of the flow development upstream of the TRS section can be found in Arroyo, 2009 and Rojo, 2015.

Circumferentially averaged profiles of swirl angle and total pressure coefficient are presented in Fig.5. The figure shows that the upstream influence of the thickened vane is quite similar compared to the regular vane, although the vane has enlarged thickness. However, for the vane with a mount-recess the bump results in redistribution of the upstream circumferentially averaged total pressure, which also causes a swirl reduction in the shroud region. The blockage of the flow due to the bump implementation leads to the pressure redistribution and therefore changes the inflow pressure conditions upstream of the OGV. The bump leads to a more skewed inlet total pressure profile shown by a red plot in the right figure.

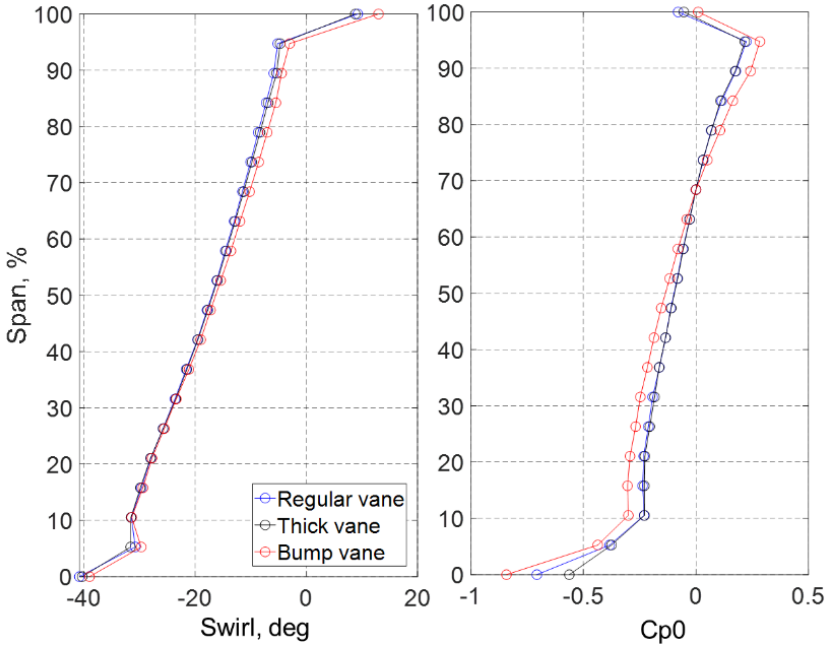

Figure 5: Circumferentially averaged inlet profiles for regular, thick and bump vanes at on-design condition.

Outlet measurements were performed for a 30-degree sector located downstream of the OGV. The circumferential resolution was 0.6˚ and radial resolution was 9.7 mm. The focus of this part of the study is on the wake comparison at on- and off-design conditions. For that reason, normalized pressure data are presented for a cropped 15-degree sector, which contains the downstream wake (Fig.6).

The secondary flow developed in the hub suction side corner is the main source of pressure losses. Therefore, the hub region is the most sensitive to the additional pressure losses. For the regular and thick vane, the wake intensity changes only for the high loading condition, which can be explained by a formation of a small separation bubble near the vane trailing edge close to the hub, which is shown by the flow visualizations in the next section of the paper. However, for the low loading case and on-design condition, there is no noticeable difference in the wake formation between regular and thick vanes.

For the bump vane, the influence of the bump is significant. It results in extra pressure losses located near the shroud, which can be seen for the on- and off-design conditions. The nature of the wake formation in the shroud region for the bump vane is different because of the interaction of the boundary layers coming from the bump as well as from the OGV. Even for the low loading case, this region with extra losses should be taken into account.

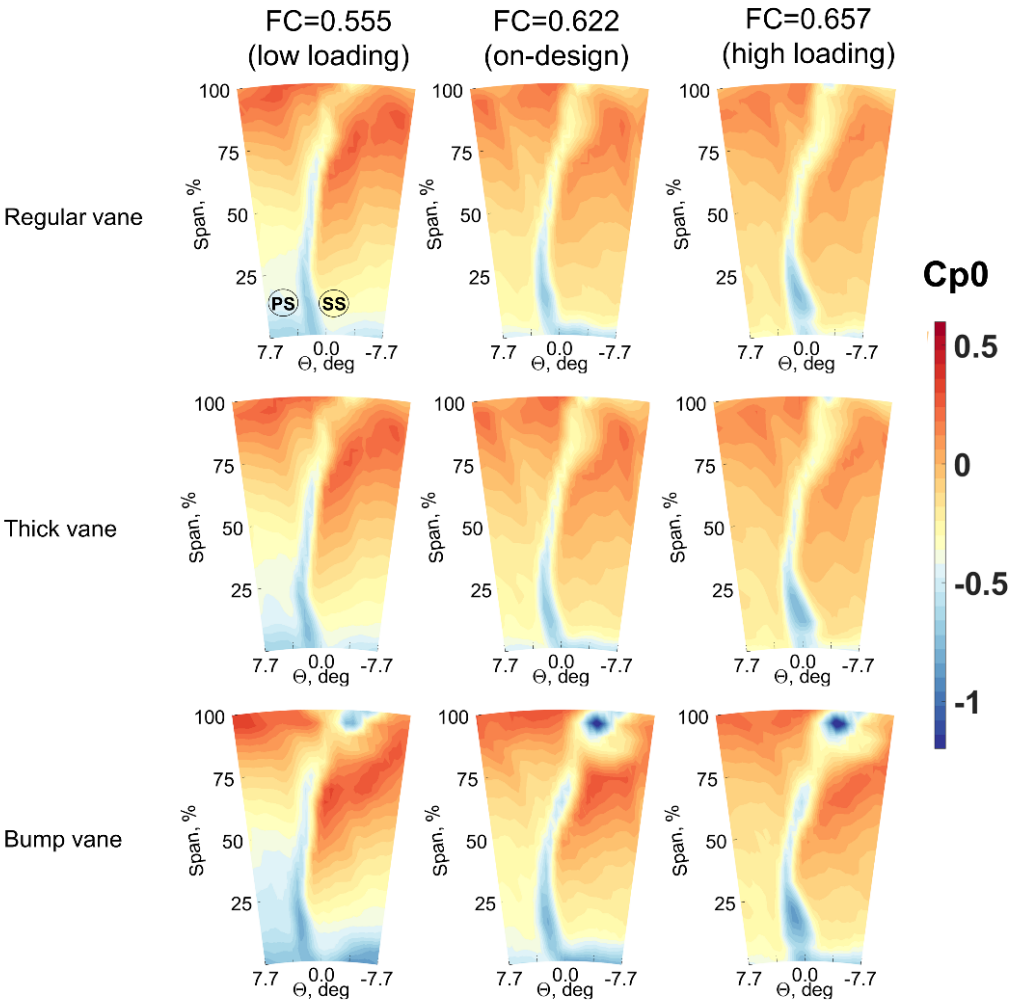

Figure 6: Outlet total pressure coefficient distributions for regular, thick and bump vanes at on- and off-design conditions

Figure 7 presents vorticity distributions at on-design conditions. Streamlines of the flow plotted using crossflow velocity components are also added to these profiles. Apart from the region of a decelerated fluid with higher vorticity values for all vanes, one can observe a well-pronounced region of the increased vorticity for the bump vane. The boundary layer developed from the bump surface has separated from the rear of the bump, as will be shown by the flow visualizations. Therefore, a strong vorticity region with decelerated fluid has been created. As can be seen, vorticity values in the core of this vortical structure are twice higher than the values in the wake region.

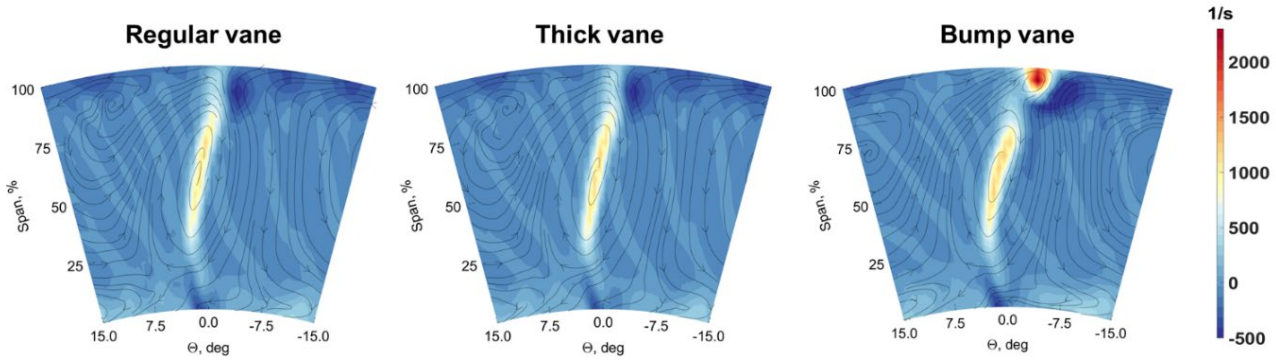

Figure 7: Downstream vorticity distributions for regular, thick and bump vanes at on-design condition

Static pressure measurements

This section presents results of the vane pressure measurements performed for regular, thick and bump vanes as well as pressure measurements on the bump surface.

The distribution of the static pressure coefficient at on-design condition is shown in Fig 8.

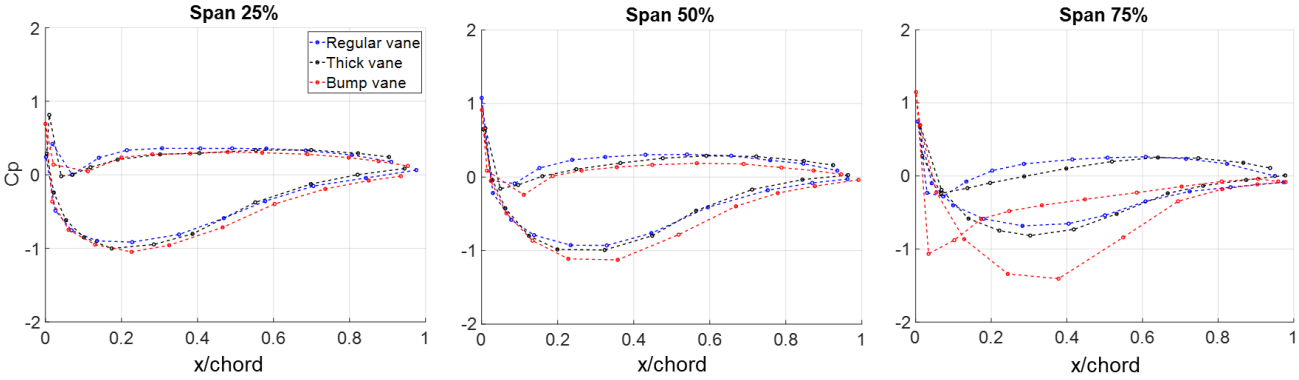

Figure 8: Static pressure distributions for regular, thick and bump vanes at on-design condition

Comparative analysis of these profiles shows that thickening of the vane, as well as presence of bump vane, creates a blockage for the passing flow. Therefore, it leads to a decrease in static pressure for the modified vanes. However, for the bump vane, the static pressure is very significantly affected at 75% span, which can be explained by the strong local influence of the bump. The flow acceleration near the front part of the bump results in much lower static pressure values both for the pressure and suction side, while the suction peak shifts downstream. Downstream flow expansion after a physical bump peak point leads to the flow deceleration. Consequently, the streamwise pressure gradient is significantly higher for the red curve from 40% chord to 70% chord.

Figure 9 presents normalized static pressure on the bump surface for different inflow conditions. For the lowest flow coefficient and, correspondingly, low loading case, a region with the lowest static pressure is located on the pressure side. For the on-design case, one can compare the previously shown profiles for the vane at 75% and the pressure distribution on the bump. As seen, the pressure minimum on the bump suction side is consistent with suction peak for the previous static pressure distribution. For the high loading case, the static pressure on the bump decreases on the vane suction side and increases on the vane pressure side. Therefore, there is a clear interaction of pressure distribution on the bump with pressure distribution on the OGV.

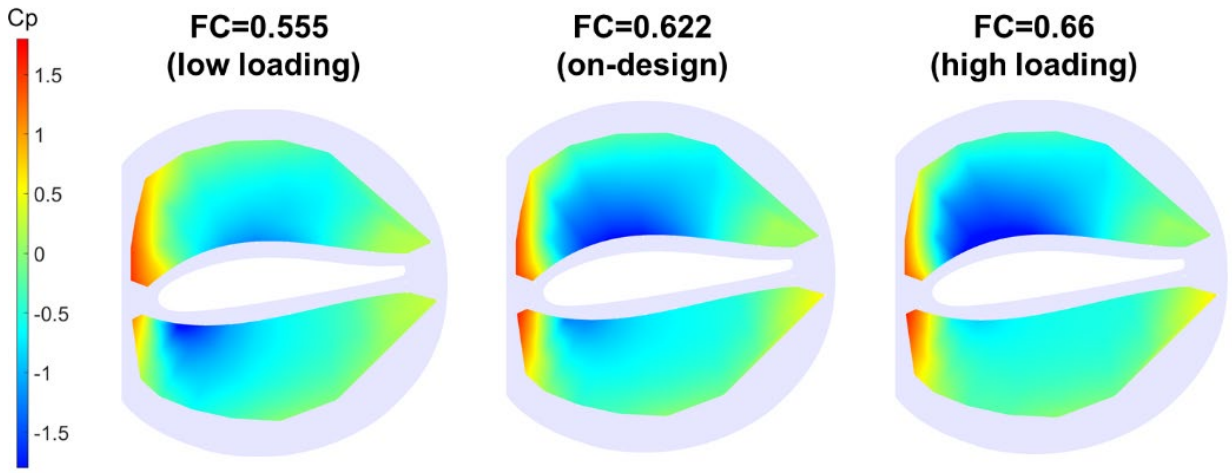

Figure 9: Static pressure distributions on the bump at on- and off-design conditions

Flow visualizations

The oil-film technique is an efficient qualitative tool in highlighting near-wall streamlines and flow separation regions. The focus of this section is on oil-film visualizations performed for thick and bump OGVs. Streamlines showing the flow development near the wall were obtained from the dynamic analysis of the flow visualization sequences and added to the visualization pictures. The results shown here are for the vane suction side at different flow coefficients. The suction side is the most influenced by the vane geometry and inlet conditions.

The flow visualizations for the thick vane are shown in Fig.10. At the off-design point with low loading, there are no flow separations, and streamlines are slightly distorted near the suction side peak due to the interplay of the radial and streamwise pressure gradients. There is also a clear streamline deviation near the hub due to the flow diffusion in the corner.

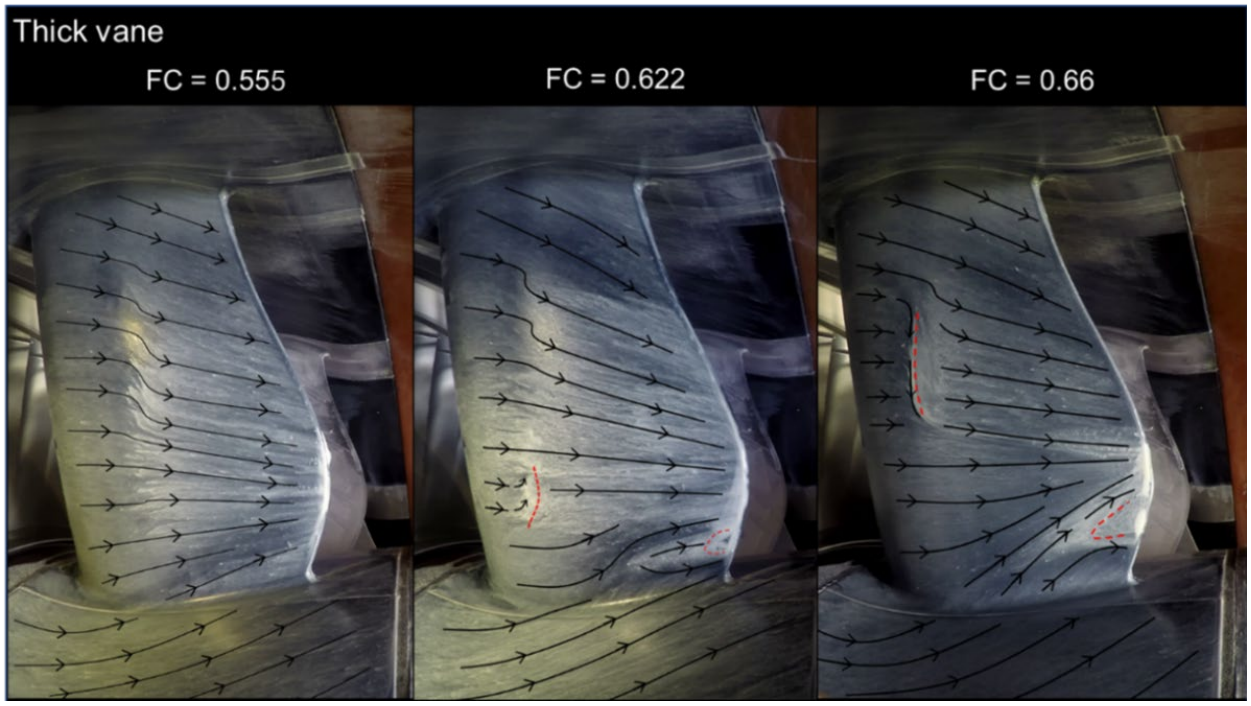

Figure 10: Oil-film visualizations for the thick vane at on- and off-design conditions

Moreover, based on visualizations on the pressure side, which are not provided here, and static pressure contours for the bump, the stagnation line is located near the leading edge without indication of any flow separations on the OGV pressure side. Increasing the load, two deceleration zones, marked with red dashed lines, are being formed. A small region located at approximately 15-20% axial chord and 25% span with concentrated powder particles reflects the presence of the flow stagnation, which can be a small separation bubble with further reattachment. In addition to this region, a small stagnation area is formed near the hub and vane trailing edge which can be explained as highly diffused interaction of the boundary layers coming from the OGV and the hub. Even for the high loading case, this region does not indicate reversed flow, while the area with accumulating particles grows and shifts towards the mid-span.

In contrast to the flow on the thick vane, for the bump vane, the flow has some pronounced differences (Fig. 11). For the on-design condition, the visualization does not indicate a clear flow stagnation in the hub corner near the vane trailing edge. However, there is a stagnation region with accumulated particles located at 20-25% of axial chord and 25% span. The location of this deceleration zone (0.45% chord) is consistent with the location of the suction peak from wall-pressure measurements. For the high loading case, this region is shifted towards the shroud as for the thick vane. As well a region with flow reversal is created in the hub corner close to the vane trailing edge, as for the thick vane.

However, the main contribution to the total pressure losses comes from a strongly decelerated flow in the shroud corner near the bump. For all three inlet conditions, one can observe that the flow near the shroud is complex and a pronounced deceleration zone is formed as the bump diffuses the flow. Moreover, this reversal flow is formed in this region, which subsequently downstream develops into a strong vortical structure visible in the downstream vorticity distribution in Fig. 7.

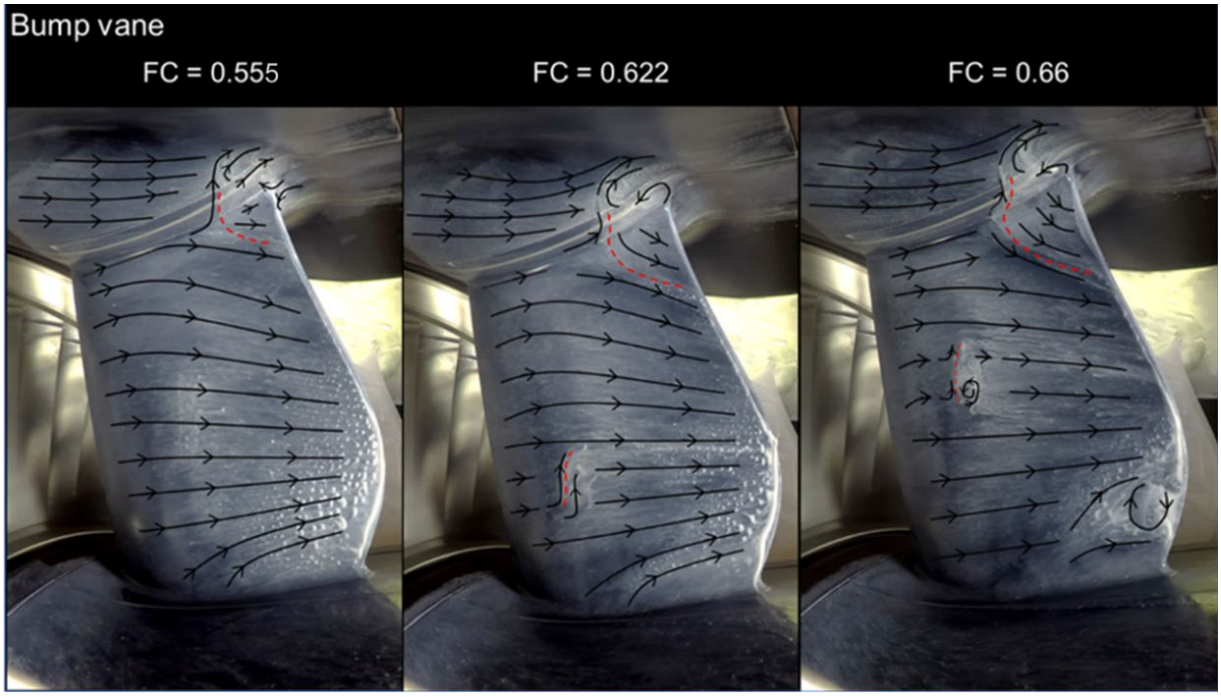

Figure 11: Oil-film visualization for the bump vane at on- and off-design conditions

CONCLUSIONS

In this paper, an engine-realistic TRS configuration with polygonal shroud design and different types of OGVs (regular, thick and bump vane) was experimentally studied for the first time. The experimental measurements, including basic aerodynamic performance and flow visualizations, were carried out at engine-representative flow Reynolds number of 350000 at on- and off-design conditions of the flow swirl angle after the upstream LPT stage.

Based on results from pressure measurements, the thickened vane is shown to have good aerodynamic performance without notable additional losses compared to the regular vane. Flow patterns obtained from the oil-film visualizations indicate two deceleration zones with small separation bubbles and further reattachment, however, does not indicate any reversal flow which proves a good vane design without loss of the turning performance.

Concerning the vane with engine-mount recess, the bump significantly influences the aerodynamics around the OGV. From circumferentially averaged profiles, it was obtained that the bump affects the inlet conditions (swirl angle and total pressure profile) thereby influencing static pressure distribution and vane loading. Blade- and bump-loading analysis shows that bump pressure distribution interacts with vane pressure distribution influenced by the bump itself and, therefore, vane and bump combination should be designed as one aerodynamic unit. The flow around the OGV with a bump is shown to be complex due to the highly diffused boundary layer from the bump. The oil-film visualizations at all three inlet conditions have revealed reversal flow and additional stagnation area in the shroud corner region.

Further downstream, the development of this flow results in an additional vorticity region with twice higher vorticity magnitude compared to the vane wake core. Moreover, for the high loading case, the bump influences the wake intensity in the hub region due to the developed reversal flow, which is confirmed by the results of oil-visualization and wake analysis. As a result, the presence of the bump leads to additional pressure losses for all presented design conditions.

ACKNOWLEDGEMENTS

The authors would like to gratefully acknowledge financial support from the NFFP (Nationella flygtekniska forskningsprogrammet) and the EU-commission. This project has received funding from the Clean Sky 2 Joint Undertaking under the European Union's Horizon 2020 research and innovation programme under grant agreement No 821398. Chalmers Laboratory of Fluids and Thermal Sciences is acknowledged for hosting the facility and for the measurement equipment. The authors would also like to acknowledge the contribution and support by GKN Aerospace Sweden.

REFERENCES

Arroyo, C., (2009). *Aerothermal Investigation of an Intermediate Turbine Duct.* PhD Thesis, Chalmers University of Technology, Gothenburg, Sweden.

Hjärne, J., Chernoray, V., Larsson, J., Löfdahl, L., (2006). *An Experimental Investigation of Secondary Flows and Loss Development Downstream of a Highly Loaded Low Pressure Turbine Outlet Guide Vane Cascade.* Proceedings of ASME Turbo Expo 2006, Paper GT2006-90561.

Hjärne, J., Chernoray, V., Larsson, J., Löfdahl, L., (2007). *Numerical Validations of Secondary Flows and Loss Development Downstream of a Highly Loaded Low Pressure Turbine Outlet Guide Vane Cascade.* Proceedings of ASME Turbo Expo 2007, Paper GT2007-27712.

Hjärne, J., Chernoray, V., Larsson, J., (2008). *Experimental Investigations and Numerical Validation of an Outlet Guide Vane with an Engine Mount Recess.* Proceedings of ASME Turbo Expo 2008, Paper GT2008-50168.

Jonsson, I., Chernoray, V., Dhanasegaran, R., (2019). *Infrared Thermography Investigation of Heat Transfer on Outlet Guide Vanes in an Engine Exit Module.* Proceedings of 13th European Turbomachinery Conference on Turbomachinery Fluid Dynamics and Thermodynamics.

Jonsson, I., Deshpande, S., Chernoray, V., Thulin, O., Larsson, J., (2020). *Experimental and Numerical Study of Laminar-Turbulent Transition on a Low-Pressure Turbine Outlet Guide Vane.* Proceedings of ASME Turbo Expo 2020, Paper GT2020-1787.

Rojo, B., Kristmundsson, D., Chernoray, V., Arroyo C., Larsson J., (2015). *Facility for Investigating the Flow in a Low Pressure Turbine Exit Structure.* Proceedings of 11th European Conference on Turbomachinery Fluid Dynamics and Thermodynamics.

Schönleiner, F., Koch, H., Selic, T., Hoeger, M., Marn A., (2014) *Comparison of the Experimental Results Between a 2D EGV Cascade Test and a Rig Test Under Engine Representative Conditions.* Proceedings of the ASME Turbo Expo 2014, Paper GT2014-26915.

Selic, T., Lengani, D., Marn, A., and Heitmeir, F., (2012*). Aerodynamic Effects of an Unshrouded Low Pressure Turbine on a Low Aspect Ratio Exit Guide Vane.* Proceedings of ASME Turbo Expo 2012, Paper No GT2012-68981.

Sonoda T., Schreiber H., Arima T., (2008). *Endwall Performance of Outlet Guide Vane Cascades With Different Blade Loading Distributions.* Proceedings of ASME Turbo Expo 2008, Paper No GT2008-51111.

Vikhorev, V., Chernoray, V., Thulin, O., Deshpande, S., Larsson, J., (2020). *Detailed Experimental Study of the Flow in a Turbine Rear Structure at Engine Realistic Flow Conditions.* Proceedings of ASME Turbo Expo 2020, Paper No GT2020-15734.